Convergence of Ubiquitylation and Phosphorylation Signaling in Rapamycin-treated Yeast Cells*[S]

Vytautas Iesmantavicius‡, Brian T. Weinert‡, and Chunaram Choudhary‡§

The target of rapamycin (TOR) kinase senses the availability of nutrients and coordinates cellular growth and proliferation with nutrient abundance. Inhibition of TOR mimics nutrient starvation and leads to the reorganization of many cellular processes, including autophagy, protein translation, and vesicle trafficking. TOR regulates cellular physiology by modulating phosphorylation and ubiquitylation signaling networks; however, the global scope of such regulation is not fully known. Here, we used a mass-spectrometry-based proteomics approach for the parallel quantification of ubiquitylation, phosphorylation, and proteome changes in rapamycin-treated yeast cells. Our data constitute a detailed proteomic analysis of rapamycin-treated yeast with 3590 proteins, 8961 phosphorylation sites, and 2299 di-Gly modified lysines (putative ubiquitylation sites) quantified. The phosphoproteome was extensively modulated by rapamycin treatment, with more than 900 up-regulated sites one hour after rapamycin treatment. Dynamically regulated phosphoproteins were involved in diverse cellular processes, prominently including transcription, membrane organization, vesicle-mediated transport, and autophagy. Several hundred ubiquitylation sites were increased after rapamycin treatment, and about half as many decreased in abundance. We found that proteome, phosphorylation, and ubiquitylation changes converged on the Rsp5-ubiquitin ligase, Rsp5 adaptor proteins, and Rsp5 targets. Putative Rsp5 targets were biased for increased ubiquitylation, suggesting activation of Rsp5 by rapamycin. Rsp5 adaptor proteins, which recruit target proteins for Rsp5-dependent ubiquitylation, were biased for increased phosphorylation. Furthermore, we found that permeases and transporters, which are often ubiquitylated by Rsp5, were biased for reduced ubiquitylation and reduced protein abundance. The convergence of multiple proteome-level changes on the Rsp5 system indicates a key role of this pathway in the response to rapamycin treatment. Collectively, these data reveal new insights into the global proteome dynamics in response to rapamycin treatment and provide a first detailed view of the co-regulation of phosphorylation- and ubiquitylation-dependent signaling networks by this compound. ***Molecular & Cellular Proteomics 13: 10.1074/mcp.O113.035683, 1979–1992, 2014.***

Cellular growth and proliferation are coordinated with the availability of nutrients. The target of rapamycin (TOR)[1] kinase functions as a key integrator for diverse growth-stimulating and inhibitory signals originating from amino acids, energy levels, stress, oxygen, and growth factors (1). TOR is an atypical serine/threonine kinase conserved in all eukaryotes and is a critical regulator of energy-demanding processes such as protein synthesis, the cell cycle, metabolism, and autophagy (2). Dysregulation of TOR signaling has been implicated in many diseases, including cancer, neurodegenerative disorders, obesity, and diabetes. Consequently, the ability to modulate TOR signaling is of great pharmacological interest (3). Rapamycin, a potent inhibitor of TOR complex 1 (TORC1), is a clinically approved immunosuppressant drug that is used to prevent organ transplant rejection. Intriguingly, studies in yeast (4), flies (5), and worms (6) suggest that inhibition of TOR signaling extends lifespan, likely by mimicking dietary restriction. Furthermore, recent studies demonstrated, for the first time, that it is possible to increase the lifespan of mice pharmacologically by treating the mice with rapamycin (7, 8), although, it remains unclear whether rapamycin increases lifespan by delaying age-associated diseases or by slowing aging.

It is well established that posttranslational modifications (PTMs) serve as the basis for signal transduction in the cell. Advancements in mass spectrometry (MS)-based proteomics have greatly facilitated the large-scale identification and

From the ‡Novo Nordisk Foundation Center for Protein Research, Faculty of Health and Medical Sciences, University of Copenhagen, Blegdamsvej 3, 2200 Copenhagen, Denmark

⌘ *Author's Choice*—Final version full access.

Received November 1, 2013, and in revised form, June 23, 2014

Published, MCP Papers in Press, June 24, 2014, DOI 10.1074/mcp.O113.035683

Author contributions: V.I., B.T.W., and C.C. designed research; V.I. performed research; V.I., B.T.W., and C.C. analyzed data; V.I., B.T.W., and C.C. wrote the paper.

[1] The abbreviations used are: TOR, target of rapamycin; TORC1, target of rapamycin complex 1; SILAC, stable isotope labeling with amino acids in cell culture; PTM, posttranslational modification; di-Gly, di-glycine; MS, mass spectrometry; GO, Gene Ontology; SCX, strong cation exchange chromatography; NEDD, neural precursor cell expressed developmentally down-regulated protein; Art, arrestin-related trafficking adaptor.

quantification of several PTMs on a global scale (9, 10). *Saccharomyces cerevisiae* (commonly known as baker's yeast) has been widely used as a eukaryotic model organism for in-depth analysis of proteome (11), phosphoproteome (12), and acetylome (13). Many of the identified PTM sites have been shown to be conserved from yeast to mammals (14).

Conjugation of ubiquitin to its target proteins, termed ubiquitylation or ubiquitination, has numerous regulatory functions in eukaryotic cells. Proteome-wide mapping of ubiquitylation sites via mass spectrometry relies on the identification of the di-glycine (di-Gly) remnant that is derived from trypsin digestion of ubiquitylated proteins and remains conjugated to modified lysines (15, 16). We previously optimized a single-step, immunoaffinity purification method for large-scale analysis of ubiquitylated peptides (17, 18). This approach has been used successfully to identify thousands of endogenous ubiquitylation sites (17, 18) and to quantify site-specific changes in ubiquitylation in response to different cellular perturbations (19, 20). It should be mentioned that the di-Gly remnant is not absolutely specific for proteins modified by ubiquitin; proteins modified by NEDD8 (and ISG15 in mammalian cells) also generate an identical di-Gly remnant, and it is not possible to distinguish between these PTMs using this approach. However, a great majority of di-Gly modified sites originate from ubiquitylated peptides (21).

Inhibition of TOR by rapamycin results in a decrease in phosphorylation of its many direct substrates, such as transcriptional activator Sfp1 (22), autophagy-related protein Atg13 (23), and negative regulator of RNA polymerase III Maf1 (24). Notably, TOR also regulates many phosphorylation sites indirectly by activating or inactivating downstream protein kinases and phosphatases. For example, the predicted functional ortholog of the mammalian ribosomal protein S6 kinase β 1 in yeast (Sch9) is directly phosphorylated by TORC1, which in turn regulates cell cycle progression, translation initiation, and ribosome biogenesis (25). TORC1 also phosphorylates nitrogen permease reactivator 1 kinase, which has been shown to regulate cellular localization of arrestin-related trafficking adaptor 1 (Art1) (26). Art1 belongs to a family of proteins responsible for recruiting the ubiquitin ligase Rsp5, the yeast NEDD4 homolog, to its target proteins at the plasma membrane (27). Upon Art1-Rsp5-target complex formation, the target protein is ubiquitylated and degraded through ubiquitin-mediated endocytosis and trafficking to the vacuole. Thus, TORC1 coordinates downstream phosphorylation and ubiquitilation signaling in order to respond to nutrient availability. However, the global extent of rapamycin-regulated phosphorylation and ubiquitylation signaling networks is not fully known.

In this study we combined the di-Gly remnant profiling approach with phosphorylated peptide enrichment and in-depth proteome quantification in order to study protein, ubiquitylation, and phosphorylation changes induced by rapamycin treatment. Our data provide a detailed proteomic analysis of rapamycin-treated yeast and offer new insights into the phosphorylation and ubiquitylation signaling networks targeted by this compound.

MATERIALS AND METHODS

Yeast Culture and Protein Lysate Preparation—*Saccharomyces cerevisiae* cells (strain BY4742 auxotroph for lysine) were grown in a synthetic complete medium supplemented with SILAC "light" lysine (L-lysine $^{12}C_6{}^{14}N_2$), SILAC "medium" lysine (L-lysine $^{12}C_6{}^{14}N_2{}^{2}H_4$), and SILAC "heavy" lysine (L-lysine $^{13}C_6{}^{15}N_2$). At a logarithmic growth phase (A_{600} value of ~0.5), "light"-labeled yeast were mock treated, whereas "medium"- and "heavy"-labeled yeast were treated with rapamycin at 200 nM final concentration for 1 h and 3 h, respectively. Cells were harvested at 3000 × *g* for 5 min, washed twice in sterile water, resuspended in lysis buffer (50 mM Tris, pH 7.5, 150 mM NaCl, 1 mM EDTA, 1× Mini Complete protease inhibitor mixture (Roche), 5 mM sodium fluoride, 1 mM sodium orthovanadate, 5 mM β-glycerophosphate, 1 mM *N*-ethylmaleimide), frozen in liquid nitrogen, and ground using an MM400 ball mill (Retsch, Dusseldorf, Germany) for 2 to 3 min at 25 Hz. To thawed lysates, Nonidet P-40 and sodium deoxycholate were added to final concentrations of 1% and 0.1%, respectively. After centrifugation, proteins were precipitated using ice-cold acetone and resuspended in urea solution (6 M urea, 2 M thio-urea, 10 mM Hepes, pH 8.0), and the protein concentration was determined via Bradford assay.

MS Sample Preparation—Proteins extracted from "light", "medium", and "heavy" SILAC-labeled yeast were mixed in a 1:1:1 ratio, treated with 1 mM DTT for 45 min, alkylated with 5.5 mM chloroacetamide for 45 min in the dark, and digested overnight with protease Lys-C (1:100 protease-to-protein ratio). For di-Gly peptide enrichment analysis, an aliquot of the digest was further treated with modified trypsin overnight (1:100 protease-to-protein ratio). Proteases were inactivated by the addition of TFA to a final concentration of 1%, and precipitates were removed by centrifugation at 2000 × *g* for 5 min. Peptide supernatants were loaded onto reversed phase (C18) Sep-Pak cartridges (Waters, Milford, MA). Peptides from the cartridges were eluted using 4 ml of 50% acetonitrile solution, and the concentration was determined via absorbance at 280 nm using a spectrophotometer (NanoDrop 2000, Thermo Scientific). To analyze the proteome of rapamycin-treated cells, 30 μg of peptides were acidified using 1% TFA and loaded onto a strong cation exchange (SCX) microtip column prepared as described previously (28). We used an optimized protocol for micro-SCX-based fractionation (29). Briefly, the column was conditioned with 100 μl of 0.1% TFA, 50% acetonitrile, washed with 100 μl of pH 8.5 elution buffer, and equilibrated with 100 μl of 0.1% TFA, 50% acetonitrile. After loading, the microtip column was washed with 100 μl of 0.1% TFA, 50% acetonitrile, and then peptides were eluted by stepwise 100-μl aliquots of SCX buffers of pH 4.0, 4.5, 5.0, 5.5, 6.5, and 8.5. Buffers for SCX were prepared from 20 mM acetic acid, 20 mM boric acid, 20 mM phosphoric acid starting solution by adjusting to desired pH with 1 M NaOH and adjusting the final concentration of acetonitrile to 40%. To remove acetonitrile from peptide eluates, samples were briefly evaporated in a centrifugal evaporator and then desalted using C18 StageTips as described previously (30). For enrichment of di-Gly modified peptides, a PTMScan ubiquitin remnant motif kit (Cell Signaling Technology, Danvers, MA) was used. Shortly, 10 mg of peptides eluted from the Sep-Pak cartridge were supplemented with 10× immunoprecipitation buffer provided with the kit, and this was followed by 1 h of centrifugal evaporation at 45 °C in order to remove acetonitrile. The volume was adjusted to result in a 1× immunoprecipitation buffer concentration, and samples were incubated for 4 h at 4 °C with the di-Gly-lysine-specific monoclonal antibody on a rotation wheel as described previously (17). The immunoprecipitates were washed

three times with immunoprecipitation buffer, washed three times with water, and eluted with 0.1% TFA acidified water. Immunoenriched peptides were fractionated using a microtip SCX column prepared as described above. Peptides were eluted through stepwise 100-μl aliquots of SCX buffers of pH 4.5, 5.0, 5.5, 6.0, 7.0, and 8.5 followed by desalting using C18 StageTips as described previously (30). For the enrichment of phosphorylated peptides, 5 mg of peptides were acidified to a final concentration of 6% TFA (31–33) and supplemented with acetonitrile to a final concentration of 50%. 10 mg of titanium dioxide beads (10 μm, Titansphere, GL Sciences, Tokyo, Japan) were washed once with 6% TFA, 50% acetonitrile solution, transferred to a tube containing acidified peptides, and incubated for 1 h on a rotating wheel at room temperature. The beads were washed twice with 0.5 ml of 6% TFA in 50% acetonitrile and then twice with 0.5 ml of 0.1% TFA in 50% acetonitrile and transferred onto a C8 packed StageTip. The bound phosphorylated peptides were eluted using 100 μl of 5% NH_4OH followed by 100 μl of 10% NH_4OH in 25% acetonitrile. The eluates were combined, and ammonia was removed by centrifugal evaporation at 45 °C. The peptides were acidified and loaded onto a microtip SCX column as described above. For the elution of phosphopeptides, buffers with the following pH values were used: 3, 3.5, 4, 5, 7, and 11. Acetonitrile from the eluent was removed by centrifugal evaporation for 15 min at 45 °C followed by desalting using C18 packed StageTips.

LC-MS/MS Analysis—Peptides were eluted from the StageTips using 40 μl of 40% acetonitrile in 0.5% acetic acid solution and analyzed on an EASY-nLC system (Thermo Scientific) connected to a Q-Exactive (Thermo Scientific) mass spectrometer. A 15-cm column of 75-μm diameter packed with 3-μm beads (Reprosil-AQ Pur, Dr. Maisch, Ammerbuch-Entringen, Germany) was used to separate the peptides at a flow rate of 250 nl/min. The liquid was directly electrosprayed using a spray voltage of 2 kV and a heat capillary temperature of 275 °C. The mass spectrometer was operated using Xcalibur 2.2 in the data-dependent acquisition mode with up to 12 of the most intense peaks selected for fragmentation using higher collisional dissociation for all MS/MS events as described previously (34, 35). In order to avoid repeated sequencing of the same peptides, a dynamic exclusion window of 30 s was used. Full scans were acquired in the *m/z* range of 300–1750 with a target value of 1e6 ions, a maximum injection time of 120 ms, and $r = 70{,}000$ at *m/z* 400. For the fragmentation spectrum, a maximum of 1e5 ions were selected with an isolation window of 2.5 Da and a minimum signal intensity of 5e4. The resolution was set at $r = 17{,}500$ at *m/z* 400 for whole proteome measurements with a maximum injection time of 64 ms, whereas for phosphoproteome and ubiquitylome measurements $r = 35{,}000$ at *m/z* 400 and a maximum injection time of 128 ms were used. MS/MS peaks with an unknown charge state or a charge state of 1 were not selected. In addition, for di-Gly-modified peptides, charge states of 2 were also excluded.

Computational Analysis of MS Data—Raw mass spectrometry data files were analyzed using MaxQuant version 1.3.3.2 with the integrated Andromeda search engine (36, 37). Peptides were identified by searching parent ion and fragment spectra against the Saccharomyces Genome Database, genome release r63, containing 6717 putative protein sequences (forward and reversed database supplemented with common contaminants). The initial search was performed using a mass tolerance of 20 ppm and was followed by mass recalibration and the main search with a mass tolerance of 6 ppm for parent ions and 20 ppm (higher collisional dissociation) for fragment ions. Peptide sequences were searched using trypsin specificity and allowing a maximum of two missed cleavages. Cystein carbamidomethylation, cysteine N-ethylmaleimidation, N-acetylation of proteins, and oxidized methionine were search as variable modifications for all raw files, whereas di-Gly modification of lysine and phosphorylation of serine, threonine, and tyrosine were searched as variable modifications where relevant. The false discovery rate was estimated using a target-decoy approach (38) allowing a maximum of 1% false identifications from a reversed sequence database. Only high-confidence sites were considered in this study, defined as those having a localization probability of more than 0.75 for phosphorylated peptides and 0.90 for di-Gly modified peptides, a posterior error probability score less than 0.01, and an Andromeda score difference between the best and second best peptide match of more than 5. MS/MS spectra for proteins identified by a single unique peptide (MS2 PDF proteins), MS/MS spectra for phosphorylated peptides (MS2 PDF phosphorylation), and MS/MS spectra for ubiquitylated peptides (MS2 PDF ubiquitylation) have been provided as supplemental data with references to the unique identification numbers provided in tables for protein groups (supplemental Table S2), phosphorylation sites (supplemental Table S3), and ubiquitylation sites (supplemental Table S5).

Data Analysis—Statistical significance was calculated using the R environment. Gene Ontology (GO) term association and enrichment analysis were performed using the Database for Annotation, Visualization and Integrated Discovery (DAVID) (39). Phosphorylation and di-Gly-modified sites were clustered based on their dynamic behavior using GProx (40). Amino acid motif enrichment within clusters was analyzed using IceLogo (41). To construct a protein–protein interaction network, the STRING database system was used (42). Functional protein interaction networks were visualized using Cytoscape (43).

RESULTS

Experimental Strategy—In this study we analyzed rapamycin-induced changes in protein, ubiquitylation, and phosphorylation abundance at two time points (1 h and 3 h) in the model organism *S. cerevisiae* (Fig. 1*A*). Proteome changes were quantified in an unbiased (non-hypothesis-driven) manner using a SILAC-based proteomic approach (44). Protein extracts from "light" (control, mock treated), "medium" (1 h, 200 nM rapamycin), and "heavy" (3 h, 200 nM rapamycin) SILAC-labeled yeast samples were combined in equal amounts and digested to peptides using Lys-C and trypsin. Di-Gly-modified peptides were enriched using a monoclonal antibody directed toward the di-Gly remnant (16, 17, 21). Phosphorylated peptides were enriched using TiO_2-based metal affinity chromatography (32, 33). In order to reduce sample complexity, peptides were fractionated using microtip SCX columns (28, 45). Peptides were analyzed by means of high-pressure nano-flow reversed phase chromatography directly connected to a quadrupole-Orbitrap mass spectrometer (Q Exactive) (34, 35). Computational analysis of MS data was performed using MaxQuant (36, 37), allowing a maximum false discovery rate of 1%. We used stricter criteria for PTM analysis by requiring a minimum posterior error probability score of 0.01 and localization probability of 0.75 for phosphorylated peptides or 0.9 for di-Gly-modified peptides. From three biological replicates, we quantified 3590 proteins, 2299 di-Gly modification sites, and 8961 phosphorylation sites (supplemental Table S1).

The Rapamycin-regulated Proteome—In order to provide an in-depth proteomic analysis of rapamycin-treated yeast cells, we sought to quantify changes in protein abundance.

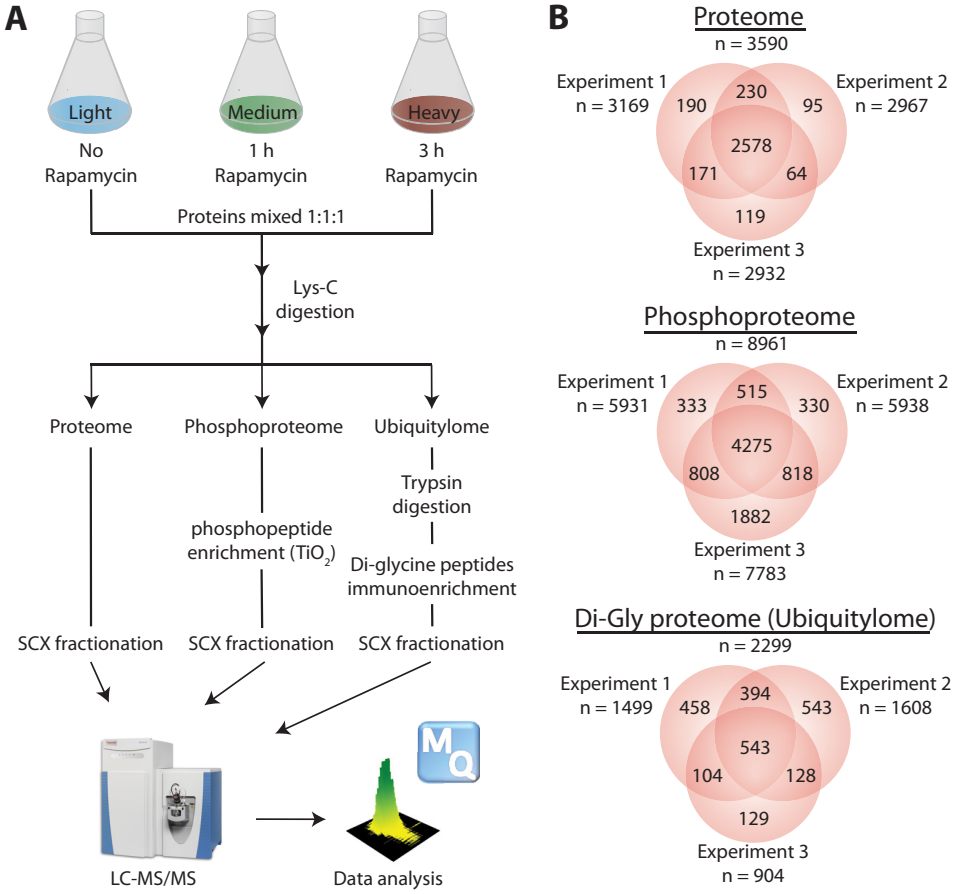

FIG. 1. **Proteome, phosphoproteome, and ubiquitylome analysis of rapamycin-treated yeast.** *A*, experimental outline. Exponentially growing yeast cells were metabolically labeled with lysine^0 (light), lysine^4 (medium), or lysine^8 (heavy). Rapamycin was added to 0.2 mM, and cells were harvested at the indicated time points. Equal amounts of proteins were mixed and digested under denaturing conditions using endoproteinase Lys-C. Phosphorylated peptides were enriched using TiO_2-based chromatography, and di-Gly-modified (ubiquitylated) peptides were enriched using anti-di-Gly monoclonal antibody. All peptides were fractionated with micro-SCX prior to analysis using reversed phase liquid chromatography–tandem mass spectrometry (LC-MS/MS). *B*, overlap between biological replicates for proteome, phosphoproteome, and ubiquitylome. The Venn diagrams indicate the number (*n*) of sites or proteins identified in each experiment and the overlap between biological replicates.

Furthermore, by determining the protein abundance in rapamycin-treated yeast, we were able to more accurately quantify changes occurring at PTM levels by correcting changes in PTM abundance for changes in protein abundance. In total, 3590 proteins were quantified with at least two ratio counts, of which 2578 were observed in all three biological replicates (Fig. 1*B* and supplemental Table S2). PTM changes were corrected for changes in protein abundance if possible; otherwise the uncorrected PTM changes were used for further analysis. SILAC ratio changes were significantly correlated between experimental replicates at both time points, and the correlation increased at the 3-h time point when the proteome was more substantially regulated (supplemental Figs. S1*A* and S1*B*). Proteins whose SILAC ratios deviated more than two standard deviations (δ) from the median at the 1-h time point were considered as significantly regulated upon rapamycin treatment. Applying these criteria, we found that 77 and 253 proteins were significantly up-regulated and 69 and 147 proteins were significantly down-regulated after 1 h and 3 h of rapamycin treatment, respectively (Fig. 2*A* and supplemental Table S2). To further validate the quantitative MS findings, we verified protein abundance changes in three proteins via immunoblot analysis (supplemental Fig. S1*C*). Protein abundance was significantly increased for proteins encoded by genes that were previously shown (46) to be up-regulated by rapamycin treatment (supplemental Fig. S1*D*). However, down-regulated gene expression was not associated with decreased protein abundance, suggesting that the reduced protein abundances observed in our study might have been resulted through a post-transcriptional mechanism. GO enrichment analysis (Fig. 2*B*) showed enrichment for terms that were consistent with the ability of rapamycin to mimic nutrient deprivation. Proteins with increased abundance were associated with the terms "cellular response to stress" and "cellular amino acid biosynthetic process." Nearly one-third of the proteins with decreased abundance were associated with the

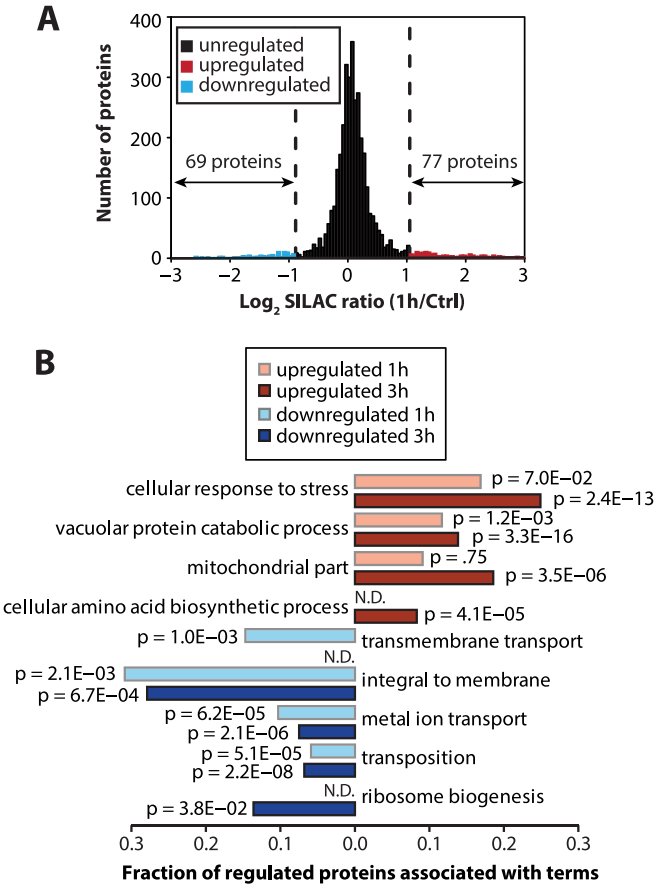

FIG. 2. **The rapamycin-regulated proteome.** *A*, identification of significantly regulated proteins. The column chart shows the distribution of SILAC ratios comparing rapamycin-treated cells (1 h) to control cells. A cutoff for significantly up- or down-regulated proteins was determined using two standard deviations from the median of the distribution. Proteins that were significantly up- or down-regulated are marked in red and blue, respectively. *B*, functional annotation of the rapamycin-regulated proteome. The bar chart shows the fraction of regulated proteins that were associated with GO terms that were significantly overrepresented among the down-regulated (blue) or up-regulated (red) proteins. Significance (*p*) was calculated with hypergeometric test.

term "integral to membrane," suggesting a specific reduction in membrane-associated proteins.

Analysis of the Rapamycin-regulated Phosphoproteome—We quantified 8961 high-confidence phosphorylation sites (referred to as class I sites with a localization probability > 0.75) in rapamycin-treated cells (Fig. 1*B* and supplemental Table S3); ~86% of these sites were corrected for changes in protein abundance, providing a more accurate measure of phosphorylation changes at these positions. Phosphorylation changes were significantly correlated between experimental replicates (supplemental Fig. S2*A*). We quantified nearly four times as many phosphorylation sites as previously reported in the largest rapamycin-regulated phosphoproteome dataset (47), although we identified only 30% of the previously identified sites (supplemental Fig. S2*B*). The relatively low overlap between these two studies likely reflects the use of different yeast strains, time points, proteases (Lys-C *versus* trypsin), digestion strategies (in-gel *versus* in-solution), and phosphopeptide enrichment strategies (IMAC *versus* TiO_2) in these studies, as well as the stochastic nature of phosphorylated peptide identification. Despite these differences, our data were significantly correlated (Spearman's correlation of 0.40, *p* value of 2.2e-16) with those of the previous study (supplemental Fig. S2*C*), providing additional confidence in the phosphorylation changes identified in our screen. The distribution of phosphorylation site ratios comparing rapamycin-treated cells to untreated cells was much broader than the distribution of unmodified peptides, suggesting extensive regulation of the phosphoproteome (Fig. 3*A* and supplemental Fig. S2*D*).

In order to determine significant changes in phosphorylation, we derived a SILAC ratio cutoff based on the distribution of SILAC ratios of unmodified peptides. SILAC ratio changes that were greater than, or less than, two standard deviations from the median for unmodified peptides were considered significant. This resulted in a SILAC ratio cutoff of 1.99 for up-regulated sites and 0.52 for down-regulated sites. These cutoff values are similar in magnitude to the typical cutoff of 2-fold change used in many SILAC-based quantitative proteomic studies. Using ratio changes that were corrected for differences in protein abundance, we found that 918 and 1431 phosphorylation sites were significantly up-regulated after 1 h and 3 h of rapamycin treatment, respectively, and that 371 and 1383 phosphorylation sites were significantly down-regulated at these time points (Fig. 3*A* and supplemental Fig. S2*D*). These data indicate that phosphorylation was already increased on a large number of sites within 1 h after rapamycin treatment, whereas the decrease in phosphorylation was more pronounced after 3 h (supplemental Fig. S2*E*). Nearly one-third of the entire phosphoproteome was regulated after 3 h of rapamycin treatment, with similar numbers of up- and down-regulated sites. Differences in protein abundance accounted for ~16% and 18% of the up-regulated and 11% and 14% of the down-regulated phosphorylation changes at the 1-h and 3-h time points, respectively (supplemental Fig. S2*F*), demonstrating that most changes occurred at the PTM level. We compared GO term enrichment for up-regulated and down-regulated phosphoproteins at both time points (supplemental Fig. S2*G*). Up-regulated phosphorylation was significantly enriched on proteins associated with the terms "transcription," "positive regulation of gene expression," "response to nutrient levels," and "autophagy." Down-regulated phosphorylation occurred on proteins associated with the terms "cell cycle," "M phase," and "site of polarized growth," and these terms were more significantly enriched at the 3-h time point, suggesting that down-regulation of phosphorylation might have resulted from reduced cell division.

To identify proteins with similar regulation, we clustered quantified phosphorylation sites according to their temporal

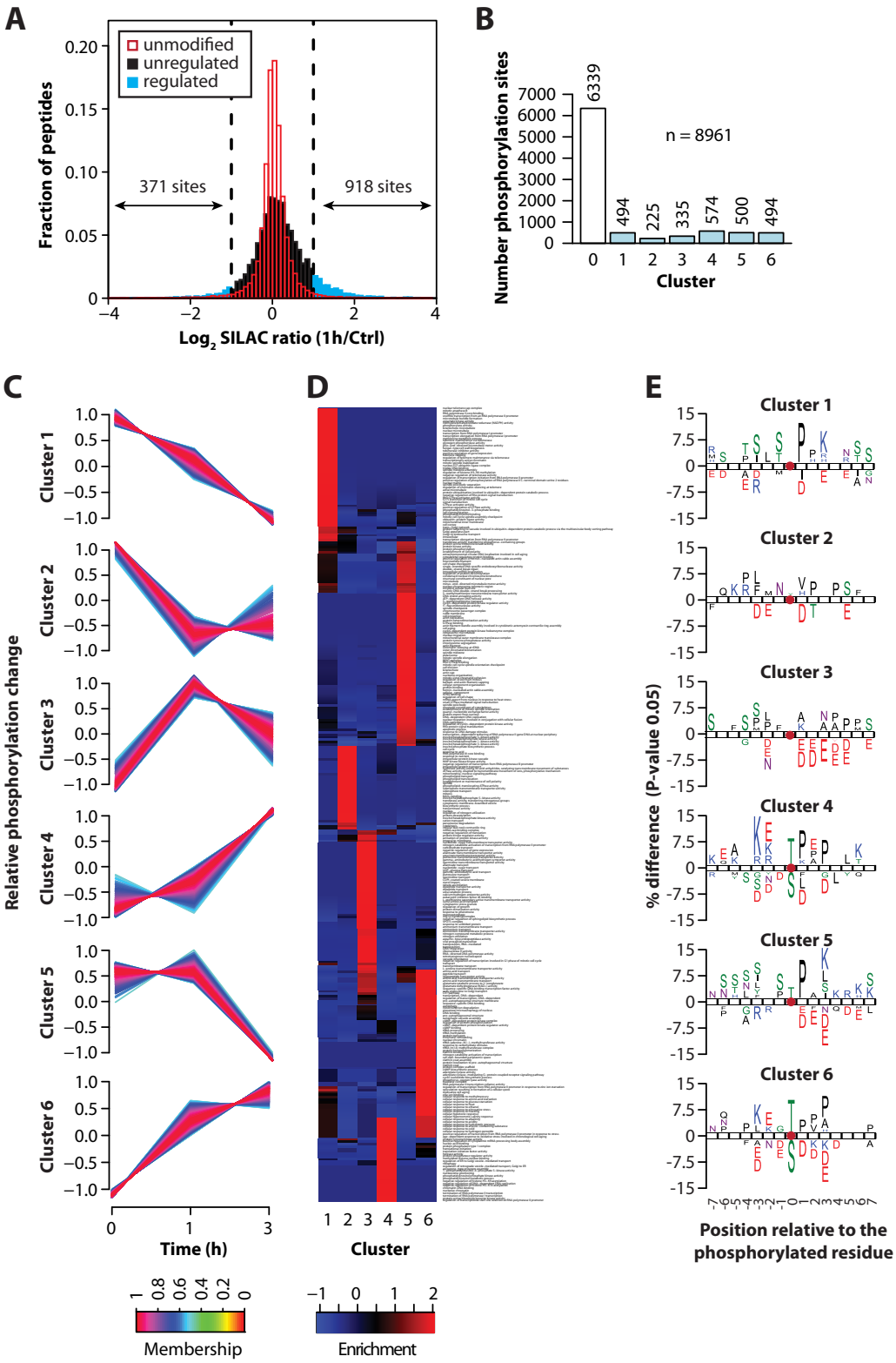

FIG. 3. **Dynamics of the rapamycin-regulated phosphoproteome.** *A*, identification of significantly regulated phosphorylation sites. The histogram shows the distribution of phosphorylation site SILAC ratios for 1h rapamycin/control (1h/ctrl) and the distribution of unmodified peptide SILAC ratios (red). The cutoff for regulated phosphorylation sites was determined based on two standard deviations from the median for unmodified peptides. Unregulated sites are shown in black, and regulated sites are shown in blue. The numbers of down-regulated and up-regulated phosphorylation sites is indicated. *B*, the bar chart shows the distribution of phosphorylation sites into seven clusters, where

behavior using a fuzzy c-means algorithm (Figs. 3*B* and 3*C*) (40, 48). Regulated phosphorylation sites were clustered into six distinct profiles based on the temporal behavior of these sites. Distinct associations of GO terms within each cluster (Fig. 3*D* and supplemental Figs. S2*H*–S2*M*) indicated that phosphorylation sites with specific temporal profiles were involved in the regulation of different biological processes. Cluster 1 included sites that showed decreased phosphorylation over the time period of our experiment. This cluster included GO terms such as "signal transduction," "ubiquitin-protein ligase activity," and "positive regulation of gene expression" (supplemental Fig. S2*H*). Consistent with this, it encompassed known regulated phosphorylation sites such as Thr142 of the transcriptional activator Msn4, which has been shown to decrease in response to osmotic stress (49), and Ser530 on the deubiquitylase Ubp1, a known Cdk1 substrate (50). This cluster also included several other interesting proteins, such as Gcd1, the γ subunit of the translation initiation factor eIF2B; Pol1, the catalytic subunit of the DNA polymerase I α-primase complex; Swi1, the transcription factor that activates transcription of genes expressed at the M/G1 phase of the cell cycle; and Atg13, the regulatory subunit of the Atg1p signaling complex that stimulates Atg1p kinase activity and is required for vesicle formation during autophagy and cytoplasm-to-vacuole targeting. In contrast, cluster 6 contained sites at which phosphorylation increased over the time period of our experiment. This cluster was enriched in GO terms related to nutrient deprivation, such as "cellular response to amino acid starvation," "amino acid transport," "autophagy," and "autophagic vacuole assembly" (supplemental Fig. S2*M*). It included phosphorylation sites on proteins such as Rph1, Tod6, Dot6, Stb3, and Par32, which have previously been shown to be hyperphosphorylated after rapamycin treatment (51). Clusters 4 and 5 showed increases and decreases in phosphorylation, respectively, suggesting that these phosphorylation sites are possibly regulated as a consequence of changes downstream of TOR inhibition, for example, by regulating the activity of downstream kinases and phosphatases upon rapamycin treatment. Clusters 2 and 3 contained sites at which the directionality of phosphorylation dynamics switched over time, suggesting that these sites might be subject to a feedback regulation or controlled by a complex regulatory program.

IceLogo (41) was used to analyze sequence motifs within the regulated phosphorylation site clusters (Fig. 3*E*). TOR kinase has a strong preference for proline in the +1 position (52), and as expected, upon rapamycin treatment a bias for proline-directed sequences was seen in clusters 1 and 5, which contained down-regulated sites. Within these clusters we found potential autophosphorylation sites on the TORC1 subunits Kog1 and Tco89. Enrichment analysis for GO biological process terms overrepresented in these clusters revealed many terms related to telomere modifications, cell cycle, and DNA replication (Fig. 3*D*). For the clusters that contained up-regulated phosphorylation sites, distinguishably different sequence motif enrichment was observed, suggesting that these sites may be targeted by kinases that are inhibited by TOR. However, TORC1 has also been implicated in association with many of the overrepresented GO terms, such as "autophagy," "ribophagy," "cellular response to various abiotic stimuli," and "CVT pathway."

In order to obtain a better understanding of the effect of PTMs on protein function, it is advantageous to determine the stoichiometry of modification. Previous work has shown that it is possible to estimate PTM stoichiometry by measuring the relative changes in modified and unmodified corresponding peptides (53). If the abundance of a posttranslationally modified peptide is substantially altered, then the abundance of the corresponding peptide will be inversely affected. Because our dataset included in-depth analysis of both proteome and phosphorylation changes, we could estimate the stoichiometry of phosphorylation. Such estimates can be inaccurate if they are based on small differences in the abundance of posttranslationally modified peptides or corresponding peptides. In order to provide a list of sites with high-confidence stoichiometry estimates, we filtered our results to ensure that the ratio of estimated stoichiometry between untreated and rapamycin-treated samples did not vary by more than 2-fold from the SILAC ratios at both time points. Using these criteria, we determined stoichiometry at 468 phosphorylation sites (supplemental Table S4), and these data identified several putative regulatory sites that undergo large changes in phosphorylation stoichiometry in response to rapamycin treatment. Serine/threonine-protein kinase Atg1 is essential for autophagy and is regulated by TOR (1); we found that Ser384 had a stoichiometry of modification that was ~10% in untreated cells and ~60% to 70% in rapamycin-treated cells, suggesting that phosphorylation at this position may play an important role in regulating Atg1 function. Isw1, the ATPase subunit of the imitation-switch chromatin remodeling complex, acts to repress stress-induced gene expression (54). We found that a phosphorylated peptide (containing Ser688, Thr689, and Ser691) on Isw1 increased from ~15% stoichiometry in untreated cells to ~50% stoichiometry after 1 h of rapamycin treatment and ~80% stoichiometry after 3 h of

cluster zero represents unregulated sites. The clusters were generated through unsupervised clustering of SILAC ratios with the fuzzy c-means algorithm. *C*, six distinct temporal patterns were generated, and the match between the profile of the cluster and phosphorylation change is described by the membership value. *D*, the heatmap shows the clustering of GO terms associated with the temporal clusters from *C*. A more detailed description of the enriched GO terms is provided in supplemental Figs. S2*H*–S2*M*. *E*, sequence motifs for distinct clusters were generated using IceLogo and show the percent difference in amino acid frequency relative to unregulated sites at a *p* value cutoff of 0.05.

rapamycin treatment, suggesting that these sites might be important for inactivating Isw1 to induce the expression of stress-activated genes. DNA polymerase α subunit B (Pol12) is an essential gene that is required for the initiation of DNA replication during mitotic and pre-mitotic DNA synthesis (55). We found that Ser100 and 101 were ~70% phosphorylated in untreated cells, and phosphorylation was decreased to ~45% and ~23% after 1 and 3 h of rapamycin treatment, respectively, indicating that phosphorylation at these positions might be important for the activity of Pol12 in initiating DNA replication, which is presumably inhibited in rapamycin-treated cells.

Analysis of the Rapamycin-regulated Ubiquitylome—In this study we quantified 2299 di-Gly-modified lysines, providing an in-depth analysis of the ubiquitylation changes in rapamycin-treated yeast (Fig. 1*B* and supplemental Table S5). A vast majority (~93%) of the quantified sites were corrected for differences in protein abundance, and as with phosphorylation, only a small fraction of the observed changes in ubiquitylation could be attributed to changes in protein abundance (supplemental Fig. S3*A*). SILAC ratio changes were well correlated between experimental replicates (supplemental Fig. S3*B*). The cutoff for identifying significantly changed ubiquitylation sites was calculated based on the distribution of unmodified peptides (Fig. 4*A* and supplemental Fig. S3*C*). 204 and 377 sites were significantly up-regulated, and 69 and 198 sites were significantly down-regulated, after 1 h and 3 h of rapamycin treatment, respectively (supplemental Fig. S3*D* and supplemental Table S5), indicating that the fraction of up-regulated sites was 2- to 3-fold larger than that of down-regulated sites at both time points. We compared GO term enrichment among proteins that showed up- or down-regulated ubiquitylation at both time points (supplemental Fig. S3*E*). The most significantly enriched terms associated with up-regulated ubiquitylation were "ribosome" and "posttranscriptional regulation of gene expression," suggesting a role for ubiquitylation in regulating protein translation or ribophagy. A majority of the down-regulated ubiquitylation sites were present on proteins that were highly significantly associated with the term "intrinsic to membrane," with smaller fractions of down-regulated ubiquitylation sites occurring on proteins associated with the terms "vacuole," "ion transport," and "amino acid transport." These data indicate globally reduced ubiquitylation of membrane proteins, possibly linked to the known role of ubiquitylation in regulating membrane protein trafficking (56).

As with phosphorylation, we clustered ubiquitylation sites based on their temporal profile. However, because the number of quantified ubiquitylation sites was much smaller than the number of phosphorylation sites, only four clusters were chosen for temporal description of the data (Figs. 4*B* and 4*C*). Distinct GO terms were associated with distinct temporal clusters, indicating that ubiquitylation sites that were similarly regulated over time affected distinct biological processes (Fig. 4*D* and supplemental Fig. S3*F*). Cluster 1 contained sites that showed increased ubiquitylation after the rapamycin treatment. This cluster included the general amino acid permease Gap1, on which TORC1-dependent, Rsp5-mediated ubiquitilation has been described previously (57), and the Rsp5 adaptor protein Bul1, which is required for Gap1 ubiquitylation. There were a number of other proteins related to the ubiquitin modification machinery present in this cluster, such as the ubiquitin conjugating enzyme Ubc6, the deubiquitylase Ubp14, the ubiquitin chain assembly factor Ufd2, and the ubiquitin binding protein Cue5. Cluster 1 also contained the human tumor suppressor NPRL2 homolog, Npr2, which is known to down-regulate TORC1 activity (58), and the chaperones Pex19, Cns1, and Ccs1, which are required for optimal translation under nutrient stress conditions (59). Clusters 3 and 4 included sites that were down-regulated in ubiquitylation upon rapamycin treatment. Cluster 3 was enriched for the GO terms "amino acid transport," "cation transport," and related terms, and cluster 4 was enriched for the terms "integral to membrane," "vacuole," and "trans-Golgi network vesicle membrane" (Fig. 4*D* and supplemental Fig. S3*F*). Consistent with the GO term enrichment analysis of down-regulated ubiquitylation shown in supplemental Fig. S3*D*, these clusters were overrepresented with amino acid and nutrient permeases including Fui1, Fcy2, Mup1, Tna1, Lyp1, Dip5, Gnp1, Can1, Hip1, Sam3, and Sge1 and membrane transporters Flc1, Cot1, Smf1, Itr2, Ymd8, Zrt2, Pho90, Arn2, Itr1, Pho87, Cwh43, Fth1, Tat1, and Fun26.

In contrast to phosphorylation, sequence motif analysis did not show substantial biases for amino acids flanking ubiquitylation sites in clusters 1 and 2, in which ubiquitylation was increased (Fig. 4*E*). However, the sites present in clusters 3 and 4 showed sequence biases of a magnitude similar to that seen in the phosphorylation site logos (Fig. 3*E*), suggesting that regulation of the permeases, transporters, and membrane proteins within these clusters may involve a degree of sequence specificity.

Cross-talk between Phosphorylation and Ubiquitylation—To identify possible cross-talk between phosphorylation and ubiquitylation, we searched our data for peptides that were both ubiquitylated and phosphorylated. Among the more than ~12,400 peptides identified from phosphopeptide-enriched fractions, no di-Gly-modified peptides were found. In contrast, among the ~6800 di-Gly-enriched peptides, we found 49 peptides that had both a di-Gly remnant and a phosphorylated amino acid (supplemental Table S6). This corresponds to 0.72% of the total number of high-confidence (posterior error probability score < 0.01) peptides observed in the di-Gly-enriched fractions. Co-modified peptides occurred on proteins present in 37 protein groups, more than half of which were transmembrane transporters and permeases (supplemental Table S6). However, looking for co-modification on a single peptide restricts the analysis to relatively short amino acid sequences and, more specifically, to tryptic peptides. On

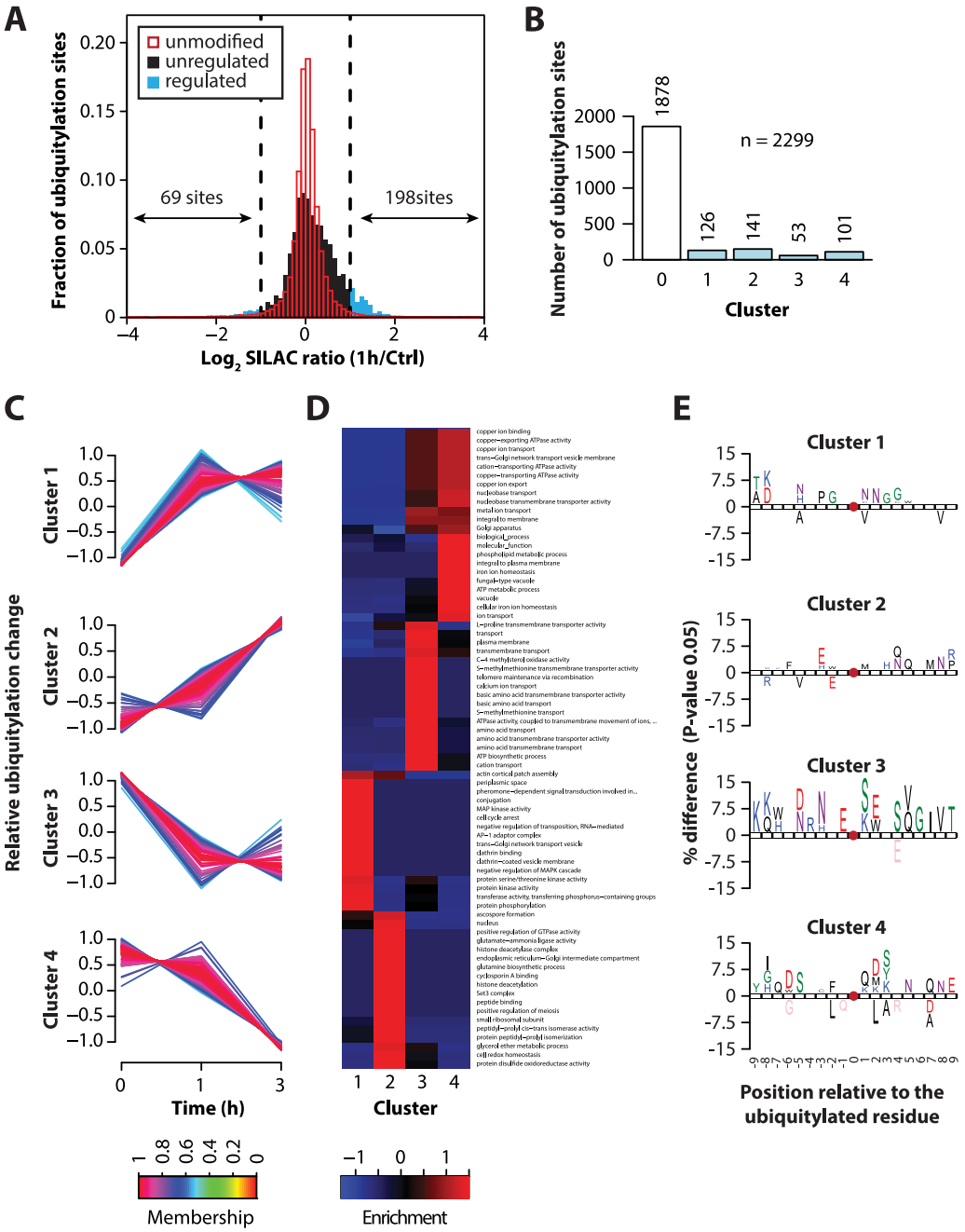

FIG. 4. **The rapamycin-regulated ubiquitylome.** *A*, identification of significantly regulated ubiquitylation sites. The histogram shows the distribution of ubiquitylation site SILAC ratios for 1h rapamycin/control (1h/ctrl) and the distribution of unmodified peptide SILAC ratios (red). The cutoff for regulated ubiquitylation sites was determined based on two standard deviations from the median for unmodified peptides. Unregulated sites are shown in black, and regulated sites are shown in blue. The numbers of down-regulated and up-regulated ubiquitylation sites is indicated. *B*, the bar chart shows the distribution of ubiquitylation sites into five clusters, where cluster zero represents unregulated sites. The clusters were generated through unsupervised clustering of SILAC ratios with the fuzzy c-means algorithm. *C*, four distinct temporal patterns were generated, and the match between the profile of the cluster and ubiquitylation change is described by the membership value. *D*, the heatmap shows the clustering of GO terms associated with the temporal clusters from *C*. A more detailed description of the enriched GO terms is provided in supplemental Fig. S3*F*. *E*, sequence motifs for distinct clusters were generated using IceLogo and show the percent difference in amino acid frequency relative to unregulated sites at a *p* value cutoff of 0.05.

the whole protein level we observed co-up-regulation by both modifications on 34 proteins after 1 h (supplemental Table S7) and 81 proteins after 3 h (supplemental Table S8). We also observed sequential modification of proteins: 31 proteins were regulated first by ubiquitylation (1-h time point) and then by phosphorylation (3-h time point) (supplemental Table S9),

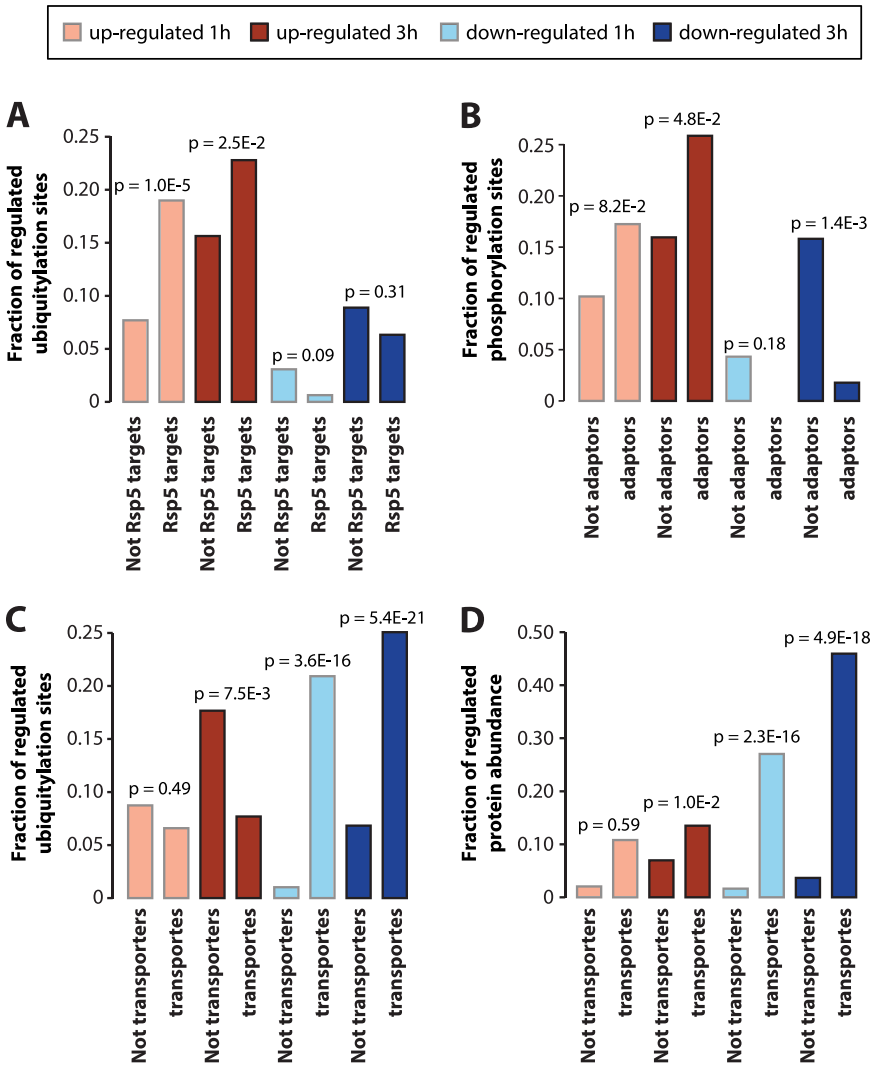

FIG. 5. **Regulation of the Rsp5 system by rapamycin.** Significantly regulated sites after 1 and 3h (see legend) were determined based on a cutoff of two standard deviations from the median for unmodified peptides. All *p* values were calculated using Fisher's exact test. *A*, the column graph compares the frequency of regulated ubiquitylation sites occurring on putative Rsp5 target proteins (Rsp5 targets) identified in Ref. 62 to all other proteins (not Rsp5 targets). *B*, the column graph compares the frequency of regulated class I phosphorylation sites occurring on the Rsp5 adaptor proteins (adaptors) Aly1, Aly2, Art5, Bul1, Bul2, Ecm21, Ldb19, Rod1, and Rog3 to all other proteins (not adaptors). *C*, the column graph compares the frequency of regulated ubiquitylation sites occurring on permeases and transporters (transporters) to all other proteins (not transporters). *D*, the column graph compares the frequency of regulated protein abundance between permeases and transporters (transporters) and all other proteins (not transporters).

and 52 proteins were regulated first by phosphorylation (1-h time point) and then by ubiquitylation (3-h time point) (Table S10). These data can serve as a useful resource for studying how phosphorylation and ubiquitylation might interact to regulate protein functions. In addition, the large fraction of co-modified peptides occurring on transmembrane permeases and transporters adds further evidence that phosphorylation and ubiquitylation signaling intersect on these proteins (see below).

Convergence of Phosphorylation and Ubiquitylation Signaling on the Rsp5 System—In yeast, Rsp5 is the only HECT-domain-containing NEDD4 ubiquitin ligase. Rsp5 is an essential ubiquitin ligase that functions in many diverse processes, such as mRNA export, chromatin remodeling, and the regulation of transcription (60). However, the best-studied role of Rsp5 is in sorting membrane permeases and transporters into the vacuole for proteasome-independent protein degradation (61). Gupta and co-workers used protein microarrays to identify 150 potential *in vitro* targets of Rsp5 (62). In our dataset we quantified 158 ubiquitylation sites on 54 of these proteins and found that the putative Rsp5 targets identified by Gupta *et al.* were significantly more likely to harbor up-regulated ubiquitylation sites (Fig. 5*A*). Rsp5 contains a WW domain that binds to L/PPxY motifs and facilitates the recognition of target proteins (63). However, some proteins that undergo Rsp5-dependent degradation, such as Gap1, Pma1, and Smf1, do not have an L/PPxY recognition motif, and instead their Rsp5-dependent ubiquitylation is facilitated by adaptor proteins that recruit Rsp5 to its target proteins (27). Recently, it was shown that nitrogen permease reactivator 1, a direct target of TORC1, modulates the phosphorylation state of Art1 in a TORC1-dependent manner to modulate the interaction among Rsp5, Art1, and a target protein (26). The phosphorylation state of Rsp5 adaptor proteins often determines whether a protein is targeted for vacuolar degradation. In this study we quantified 58 class I phosphorylation sites (site localization probability > 0.75) and 34 class II phosphorylation sites (site localization probability < 0.75) on 11 Rsp5 adaptor proteins (supplemental Table S11). We found that Rsp5 adap-

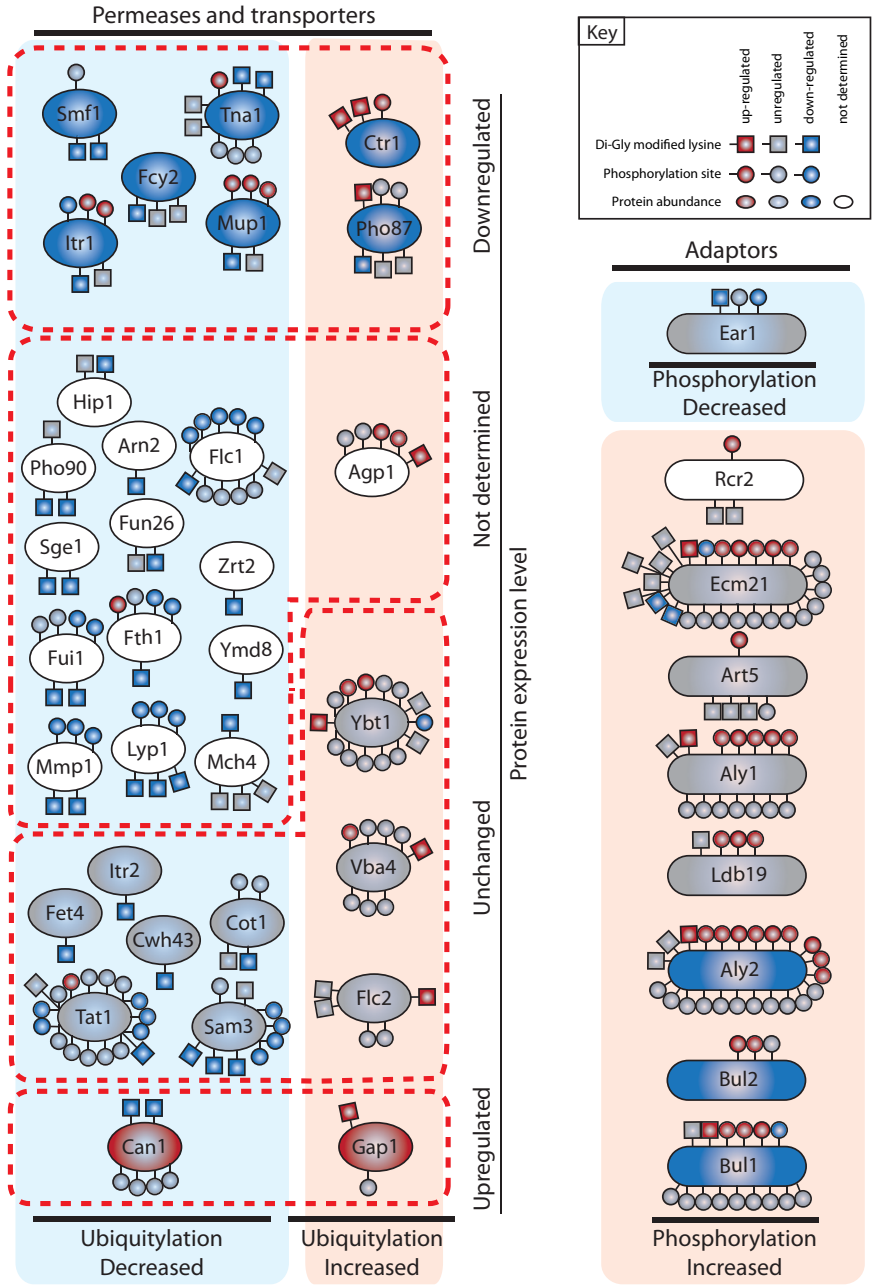

FIG. 6. **Co-regulation of permeases and transporters by ubiquitylation and phosphorylation.** The figure shows permeases, transporters, and adaptors in which ubiquitylation or phosphorylation changed significantly after 3h of rapamycin treatment. Proteins are decorated with circles and squares, which represent the number of quantified phosphorylation and ubiquitylation sites, as well as their regulation in rapamycin-treated cells as indicated in the provided color-code key. Significantly up- or down-regulated sites are indicated in red or blue, respectively. Significantly regulated proteins, phosphorylation sites, and ubiquitylation sites were identified as described in Figs. 2*A*, 3*A*, and 4*A*, respectively.

tor proteins were significantly more likely to harbor up-regulated class I phosphorylation sites in rapamycin-treated cells (Fig. 5*B*). This bias was more pronounced, and more significant, when we included the poorly localized class II sites in our analysis (supplemental Fig. S4). In accordance with the known role of Rsp5 in the regulation of subcellular localization, trafficking, and degradation of transmembrane permeases and transporters, we found that GO terms related to transporters and permeases were enriched among proteins with down-regulated ubiquitylation sites (Fig. 4*D*, supplemental Figs. S3*E* and S3*F*). Consistent with the GO analysis, we found that down-regulated ubiquitylation occurred significantly more frequently on permeases and transporters (Fig. 5*C*). In addition, we found that permease and transporter protein abundance was significantly more frequently down-regulated, although a portion of these proteins were increased in abundance (Fig. 5*D*). These data indicate that the proteome, phosphoproteome, and ubiquitylome changes induced by rapamycin treatment converge on Rsp5, Rsp5 adaptor proteins, and Rsp5 targets (Fig. 6).

DISCUSSION

The TOR kinase coordinates many aspects of cellular physiology with nutrient availability. A number of proteomic studies

have investigated phosphoproteome changes upon rapamycin treatment in yeast (47, 51) and mammalian cells (64–66). These studies provide important insights into the role of phosphorylation signaling downstream of TOR. In this study we used a multilayered proteomic approach to provide an integrated view of the rapamycin-regulated proteome, phosphoproteome, and ubiquitylome. Our data provide substantially increased coverage of rapamycin-induced phosphoproteome changes in yeast, and we provide a first global view of ubiquitylation dynamics in rapamycin-treated yeast cells. Through parallel quantification of protein abundance, we were able to normalize a vast majority of the PTM sites quantified in our study, which provided greater confidence that these changes occurred at the PTM level. Using a previously described method (53), we were able to estimate the stoichiometry at 468 phosphorylation sites, providing the first large-scale analysis of phosphorylation stoichiometry at the rapamycin-regulated sites. Many of the significantly modulated phosphorylation sites had a substantially higher stoichiometry and occurred on proteins that were previously implicated in nutrient response signaling, suggesting that these sites might have a potential regulatory function in rapamycin-modulated signaling.

The inhibition of TOR kinase by rapamycin mimics starvation, and cells respond by modulating amino acid and protein synthesis, nutrient uptake, and cell cycle progression. Analysis of GO term enrichment indicated that these processes were orchestrated in a dynamic manner on all three levels of the proteome explored in this study. A large fraction of up-regulated proteins were associated with the GO term "cellular response to stress," indicating reorganization of the proteome in response to rapamycin. The term "response to nutrient levels" was enriched on up-regulated phosphorylation sites, underlining the role of phosphorylation in regulating the stress response. Nutrient deprivation triggers the reorganization of plasma membrane proteins; in particular, nutrient transporters and permeases are targeted to vacuolar degradation. We found that the GO terms related to membrane remodeling and vacuolar trafficking were associated with regulated proteins on the proteome, phosphoproteome, and ubiquitylome levels. Our temporal analysis of these changes distinguished the immediate effects of rapamycin treatment from the changes that resulted from prolonged exposure to rapamycin and the physiological reorganization that occurs in response to TOR inhibition. In particular, we found a much greater degree of decreased phosphorylation after 3 h that was associated with GO terms related to cell growth, such as "cell cycle," "M phase," and "site of polarized growth." These general observations provide a systems-level view of the response to rapamycin and further validate our results by indicating that we were able to observe many of the expected physiological changes at the proteome, phosphoproteome, and ubiquitylome levels.

Our data showing more frequent ubiquitylation of putative Rsp5 targets, and more frequent phosphorylation of Rsp5 adaptor proteins after rapamycin treatment (Figs. 5*A* and 5*B*), suggest activation of the Rsp5 system under these conditions. Rsp5 is known to regulate the membrane localization and proteolytic degradation of transmembrane permeases and transporters by modulating their ubiquitylation. We found that permeases and transporters were biased for both reduced ubiquitylation and protein abundance, which is paradoxical to the activation of Rsp5 in rapamycin-treated cells. Although the exact reasons for this observation remain to be investigated, it is plausible that increased ubiquitylation was transient and therefore not detected at the 1-h time point, that ubiquitylated proteins were rapidly degraded, or that the degradation of these proteins is linked with deubiquitylation. Furthermore, noted changes in protein abundance may reflect biochemical accessibility rather than actual abundance, particularly for membrane proteins that may be relocalized to subcellular compartments that are biochemically inaccessible (*i.e.* detergent-insoluble fractions).

The regulation of transmembrane protein localization and vesicle sorting by Rsp5 is a complex process governed by the phosphorylation of adaptor proteins and the ubiquitylation of target proteins. The data generated in this study provide a rich resource for those wishing to understand how site-specific PTMs regulate this process. We mapped the phosphorylation sites and ubiquitylation sites that are modulated by rapamycin treatment, as well as the resultant changes in transmembrane permease and transporter abundance. We also showed that parallel mapping of phosphorylation and ubiquitylation reveals the intersection of these PTMs in regulating membrane proteins. Phosphorylation of the adaptor protein Art1 is known to regulate its function in mediating Rsp5-dependent ubiquitylation (26); our data mapping regulated phosphorylation sites on Rsp5 adaptor proteins can serve as a starting point for analyzing how phosphorylation affects the activity of these proteins. Additional studies comparing PTM dynamics in response to various stimuli could facilitate a network-level understanding of how phosphorylation and Rsp5-dependent ubiquitylation affect the fate of transmembrane permeases and transporters.

Acknowledgments—We thank the members of the Department of Proteomics at CPR for their helpful discussions. We thank the PRIDE team for helping make our data accessible to everybody. All mass spectrometry raw data associated with this manuscript have been deposited in the PRIDE data repository with accession number PXD000554.

* This work is supported by European Commission 7th Framework Program grant Proteomics Research Infrastructure Maximizing Knowledge Exchange and Access (XS) (INFRASTRUCTURESF7-2010–262067/PRIME-XS). C.C. is supported by the EMBO Young Investigator program and the Hallas Møller Investigator award from the Novo Nordisk Foundation. The Center for Protein Research is supported by a grant from the Novo Nordisk Foundation.

S This article contains supplemental material.

§ To whom correspondence should be addressed: E-mail: chuna.choudhary@cpr.ku.dk.

REFERENCES

1. Wei, Y., and Zheng, X. F. (2011) Nutritional control of cell growth via TOR signaling in budding yeast. *Methods Mol. Biol.* **759,** 307–319
2. Laplante, M., and Sabatini, D. M. (2012) mTOR signaling in growth control and disease. *Cell* **149,** 274–293
3. Dazert, E., and Hall, M. N. (2011) mTOR signaling in disease. *Curr. Opin. Cell Biol.* **23,** 744–755
4. Kaeberlein, M., Powers, R. W., 3rd, Steffen, K. K., Westman, E. A., Hu, D., Dang, N., Kerr, E. O., Kirkland, K. T., Fields, S., and Kennedy, B. K. (2005) Regulation of yeast replicative life span by TOR and Sch9 in response to nutrients. *Science* **310,** 1193–1196
5. Kapahi, P., Zid, B. M., Harper, T., Koslover, D., Sapin, V., and Benzer, S. (2004) Regulation of lifespan in Drosophila by modulation of genes in the TOR signaling pathway. *Curr. Biol.* **14,** 885–890
6. Jia, K., Chen, D., and Riddle, D. L. (2004) The TOR pathway interacts with the insulin signaling pathway to regulate C. elegans larval development, metabolism and life span. *Development* **131,** 3897–3906
7. Harrison, D. E., Strong, R., Sharp, Z. D., Nelson, J. F., Astle, C. M., Flurkey, K., Nadon, N. L., Wilkinson, J. E., Frenkel, K., Carter, C. S., Pahor, M., Javors, M. A., Fernandez, E., and Miller, R. A. (2009) Rapamycin fed late in life extends lifespan in genetically heterogeneous mice. *Nature* **460,** 392–395
8. Anisimov, V. N., Zabezhinski, M. A., Popovich, I. G., Piskunova, T. S., Semenchenko, A. V., Tyndyk, M. L., Yurova, M. N., Rosenfeld, S. V., and Blagosklonny, M. V. (2011) Rapamycin increases lifespan and inhibits spontaneous tumorigenesis in inbred female mice. *Cell Cycle* **10,** 4230–4236
9. Choudhary, C., and Mann, M. (2010) Decoding signalling networks by mass spectrometry-based proteomics. *Nat. Rev. Mol. Cell Biol.* **11,** 427–439
10. Bensimon, A., Heck, A. J., and Aebersold, R. (2012) Mass spectrometry-based proteomics and network biology. *Annual. Rev. Biochem.* **81,** 379–405
11. de Godoy, L. M., Olsen, J. V., Cox, J., Nielsen, M. L., Hubner, N. C., Frohlich, F., Walther, T. C., and Mann, M. (2008) Comprehensive mass-spectrometry-based proteome quantification of haploid versus diploid yeast. *Nature* **455,** 1251–1254
12. Bodenmiller, B., Wanka, S., Kraft, C., Urban, J., Campbell, D., Pedrioli, P. G., Gerrits, B., Picotti, P., Lam, H., Vitek, O., Brusniak, M. Y., Roschitzki, B., Zhang, C., Shokat, K. M., Schlapbach, R., Colman-Lerner, A., Nolan, G. P., Nesvizhskii, A. I., Peter, M., Loewith, R., von Mering, C., and Aebersold, R. (2010) Phosphoproteomic analysis reveals interconnected system-wide responses to perturbations of kinases and phosphatases in yeast. *Sci. Signal.* **3,** rs4
13. Henriksen, P., Wagner, S. A., Weinert, B. T., Sharma, S., Bacinskaja, G., Rehman, M., Juffer, A. H., Walther, T. C., Lisby, M., and Choudhary, C. (2012) Proteome-wide analysis of lysine acetylation suggests its broad regulatory scope in Saccharomyces cerevisiae. *Mol. Cell. Proteomics* **11,** 1510–1522
14. Beltrao, P., Albanese, V., Kenner, L. R., Swaney, D. L., Burlingame, A., Villen, J., Lim, W. A., Fraser, J. S., Frydman, J., and Krogan, N. J. (2012) Systematic functional prioritization of protein posttranslational modifications. *Cell* **150,** 413–425
15. Peng, J., Schwartz, D., Elias, J. E., Thoreen, C. C., Cheng, D., Marsischky, G., Roelofs, J., Finley, D., and Gygi, S. P. (2003) A proteomics approach to understanding protein ubiquitination. *Nat. Biotechnol.* **21,** 921–926
16. Xu, G., Paige, J. S., and Jaffrey, S. R. (2010) Global analysis of lysine ubiquitination by ubiquitin remnant immunoaffinity profiling. *Nat. Biotechnol.* **28,** 868–873
17. Wagner, S. A., Beli, P., Weinert, B. T., Nielsen, M. L., Cox, J., Mann, M., and Choudhary, C. (2011) A proteome-wide, quantitative survey of in vivo ubiquitylation sites reveals widespread regulatory roles. *Mol. Cell. Proteomics* **10,** M111.013284
18. Wagner, S. A., Beli, P., Weinert, B. T., Scholz, C., Kelstrup, C. D., Young, C., Nielsen, M. L., Olsen, J. V., Brakebusch, C., and Choudhary, C. (2012) Proteomic analyses reveal divergent ubiquitylation site patterns in murine tissues. *Mol. Cell. Proteomics* **11,** 1578–1585
19. Povlsen, L. K., Beli, P., Wagner, S. A., Poulsen, S. L., Sylvestersen, K. B., Poulsen, J. W., Nielsen, M. L., Bekker-Jensen, S., Mailand, N., and Choudhary, C. (2012) Systems-wide analysis of ubiquitylation dynamics reveals a key role for PAF15 ubiquitylation in DNA-damage bypass. *Nat. Cell Biol.* **14,** 1089–1098
20. Emanuele, M. J., Elia, A. E., Xu, Q., Thoma, C. R., Izhar, L., Leng, Y., Guo, A., Chen, Y. N., Rush, J., Hsu, P. W., Yen, H. C., and Elledge, S. J. (2011) Global identification of modular cullin-RING ligase substrates. *Cell* **147,** 459–474
21. Kim, W., Bennett, E. J., Huttlin, E. L., Guo, A., Li, J., Possemato, A., Sowa, M. E., Rad, R., Rush, J., Comb, M. J., Harper, J. W., and Gygi, S. P. (2011) Systematic and quantitative assessment of the ubiquitin-modified proteome. *Mol. Cell* **44,** 325–340
22. Lempiainen, H., Uotila, A., Urban, J., Dohnal, I., Ammerer, G., Loewith, R., and Shore, D. (2009) Sfp1 interaction with TORC1 and Mrs6 reveals feedback regulation on TOR signaling. *Mol. Cell* **33,** 704–716
23. Jung, C. H., Jun, C. B., Ro, S. H., Kim, Y. M., Otto, N. M., Cao, J., Kundu, M., and Kim, D. H. (2009) ULK-Atg13-FIP200 complexes mediate mTOR signaling to the autophagy machinery. *Mol. Biol. Cell* **20,** 1992–2003
24. Wei, Y., Tsang, C. K., and Zheng, X. F. (2009) Mechanisms of regulation of RNA polymerase III-dependent transcription by TORC1. *EMBO J.* **28,** 2220–2230
25. Urban, J., Soulard, A., Huber, A., Lippman, S., Mukhopadhyay, D., Deloche, O., Wanke, V., Anrather, D., Ammerer, G., Riezman, H., Broach, J. R., De Virgilio, C., Hall, M. N., and Loewith, R. (2007) Sch9 is a major target of TORC1 in Saccharomyces cerevisiae. *Mol. Cell* **26,** 663–674
26. MacGurn, J. A., Hsu, P. C., Smolka, M. B., and Emr, S. D. (2011) TORC1 regulates endocytosis via Npr1-mediated phosphoinhibition of a ubiquitin ligase adaptor. *Cell* **147,** 1104–1117
27. Lin, C. H., MacGurn, J. A., Chu, T., Stefan, C. J., and Emr, S. D. (2008) Arrestin-related ubiquitin-ligase adaptors regulate endocytosis and protein turnover at the cell surface. *Cell* **135,** 714–725
28. Wisniewski, J. R., Zougman, A., and Mann, M. (2009) Combination of FASP and StageTip-based fractionation allows in-depth analysis of the hippocampal membrane proteome. *J. Proteome Res.* **8,** 5674–5678
29. Weinert, B. T., Iesmantavicius, V., Wagner, S. A., Scholz, C., Gummesson, B., Beli, P., Nystrom, T., and Choudhary, C. (2013) Acetyl-phosphate is a critical determinant of lysine acetylation in E. coli. *Mol. Cell* **51,** 265–272
30. Rappsilber, J., Mann, M., and Ishihama, Y. (2007) Protocol for micro-purification, enrichment, pre-fractionation and storage of peptides for proteomics using StageTips. *Nat. Protoc.* **2,** 1896–1906
31. Zhou, H., Low, T. Y., Hennrich, M. L., van der Toorn, H., Schwend, T., Zou, H., Mohammed, S., and Heck, A. J. (2011) Enhancing the identification of phosphopeptides from putative basophilic kinase substrates using Ti (IV) based IMAC enrichment. *Mol. Cell. Proteomics* **10,** M110.006452
32. Larsen, M. R., Thingholm, T. E., Jensen, O. N., Roepstorff, P., and Jorgensen, T. J. (2005) Highly selective enrichment of phosphorylated peptides from peptide mixtures using titanium dioxide microcolumns. *Mol. Cell. Proteomics* **4,** 873–886
33. Olsen, J. V., Blagoev, B., Gnad, F., Macek, B., Kumar, C., Mortensen, P., and Mann, M. (2006) Global, in vivo, and site-specific phosphorylation dynamics in signaling networks. *Cell* **127,** 635–648
34. Kelstrup, C. D., Young, C., Lavallee, R., Nielsen, M. L., and Olsen, J. V. (2012) Optimized fast and sensitive acquisition methods for shotgun proteomics on a quadrupole orbitrap mass spectrometer. *J. Proteome Res.* **11,** 3487–3497
35. Michalski, A., Damoc, E., Hauschild, J. P., Lange, O., Wieghaus, A., Makarov, A., Nagaraj, N., Cox, J., Mann, M., and Horning, S. (2011) Mass spectrometry-based proteomics using Q Exactive, a high-performance benchtop quadrupole Orbitrap mass spectrometer. *Mol. Cell. Proteomics* **10,** M111.011015
36. Cox, J., and Mann, M. (2008) MaxQuant enables high peptide identification rates, individualized p.p.b.-range mass accuracies and proteome-wide protein quantification. *Nat. Biotechnol.* **26,** 1367–1372
37. Cox, J., Neuhauser, N., Michalski, A., Scheltema, R. A., Olsen, J. V., and Mann, M. (2011) Andromeda: a peptide search engine integrated into the MaxQuant environment. *J. Proteome Res.* **10,** 1794–1805
38. Elias, J. E., and Gygi, S. P. (2007) Target-decoy search strategy for increased confidence in large-scale protein identifications by mass spectrometry. *Nat. Methods* **4,** 207–214
39. Huang da, W., Sherman, B. T., and Lempicki, R. A. (2009) Systematic and integrative analysis of large gene lists using DAVID bioinformatics resources. *Nat. Protoc.* **4,** 44–57
40. Rigbolt, K. T., Vanselow, J. T., and Blagoev, B. (2011) GProX, a user-friendly platform for bioinformatics analysis and visualization of quantitative proteomics data. *Mol. Cell. Proteomics* **10,** O110.007450

41. Colaert, N., Helsens, K., Martens, L., Vandekerckhove, J., and Gevaert, K. (2009) Improved visualization of protein consensus sequences by iceLogo. *Nat. Methods* **6,** 786–787
42. Franceschini, A., Vilotti, S., Ferrari, M. D., van den Maagdenberg, A. M., Nistri, A., and Fabbretti, E. (2013) TNFalpha levels and macrophages expression reflect an inflammatory potential of trigeminal ganglia in a mouse model of familial hemiplegic migraine. *PLoS One* **8,** e52394
43. Cline, M. S., Smoot, M., Cerami, E., Kuchinsky, A., Landys, N., Workman, C., Christmas, R., Avila-Campilo, I., Creech, M., Gross, B., Hanspers, K., Isserlin, R., Kelley, R., Killcoyne, S., Lotia, S., Maere, S., Morris, J., Ono, K., Pavlovic, V., Pico, A. R., Vailaya, A., Wang, P. L., Adler, A., Conklin, B. R., Hood, L., Kuiper, M., Sander, C., Schmulevich, I., Schwikowski, B., Warner, G. J., Ideker, T., and Bader, G. D. (2007) Integration of biological networks and gene expression data using Cytoscape. *Nat. Protoc.* **2,** 2366–2382
44. Ong, S. E., Blagoev, B., Kratchmarova, I., Kristensen, D. B., Steen, H., Pandey, A., and Mann, M. (2002) Stable isotope labeling by amino acids in cell culture, SILAC, as a simple and accurate approach to expression proteomics. *Mol. Cell. Proteomics* **1,** 376–386
45. Weinert, B. T., Scholz, C., Wagner, S. A., Iesmantavicius, V., Su, D., Daniel, J. A., and Choudhary, C. (2013) Lysine succinylation is a frequently occurring modification in prokaryotes and eukaryotes and extensively overlaps with acetylation. *Cell Rep.* **4,** 842–851
46. Hardwick, J. S., Kuruvilla, F. G., Tong, J. K., Shamji, A. F., and Schreiber, S. L. (1999) Rapamycin-modulated transcription defines the subset of nutrient-sensitive signaling pathways directly controlled by the Tor proteins. *Proc. Natl. Acad. Sci. U.S.A.* **96,** 14866–14870
47. Soulard, A., Cremonesi, A., Moes, S., Schutz, F., Jeno, P., and Hall, M. N. (2010) The rapamycin-sensitive phosphoproteome reveals that TOR controls protein kinase A toward some but not all substrates. *Mol. Biol. Cell* **21,** 3475–3486
48. Futschik, M. E., and Carlisle, B. (2005) Noise-robust soft clustering of gene expression time-course data. *J. Bioinform. Comput. Biol.* **3,** 965–988
49. Soufi, B., Kelstrup, C. D., Stoehr, G., Frohlich, F., Walther, T. C., and Olsen, J. V. (2009) Global analysis of the yeast osmotic stress response by quantitative proteomics. *Mol. Biosyst.* **5,** 1337–1346
50. Holt, L. J., Tuch, B. B., Villen, J., Johnson, A. D., Gygi, S. P., and Morgan, D. O. (2009) Global analysis of Cdk1 substrate phosphorylation sites provides insights into evolution. *Science* **325,** 1682–1686
51. Huber, A., Bodenmiller, B., Uotila, A., Stahl, M., Wanka, S., Gerrits, B., Aebersold, R., and Loewith, R. (2009) Characterization of the rapamycin-sensitive phosphoproteome reveals that Sch9 is a central coordinator of protein synthesis. *Genes Dev.* **23,** 1929–1943
52. Linding, R., Jensen, L. J., Ostheimer, G. J., van Vugt, M. A., Jorgensen, C., Miron, I. M., Diella, F., Colwill, K., Taylor, L., Elder, K., Metalnikov, P., Nguyen, V., Pasculescu, A., Jin, J., Park, J. G., Samson, L. D., Woodgett, J. R., Russell, R. B., Bork, P., Yaffe, M. B., and Pawson, T. (2007) Systematic discovery of in vivo phosphorylation networks. *Cell* **129,** 1415–1426
53. Olsen, J. V., Vermeulen, M., Santamaria, A., Kumar, C., Miller, M. L., Jensen, L. J., Gnad, F., Cox, J., Jensen, T. S., Nigg, E. A., Brunak, S., and Mann, M. (2010) Quantitative phosphoproteomics reveals widespread full phosphorylation site occupancy during mitosis. *Sci. Signal.* **3,** ra3
54. Lindstrom, K. C., Vary, J. C., Jr., Parthun, M. R., Delrow, J., and Tsukiyama, T. (2006) Isw1 functions in parallel with the NuA4 and Swr1 complexes in stress-induced gene repression. *Mol. Cell. Biol.* **26,** 6117–6129
55. Foiani, M., Marini, F., Gamba, D., Lucchini, G., and Plevani, P. (1994) The B subunit of the DNA polymerase alpha-primase complex in Saccharomyces cerevisiae executes an essential function at the initial stage of DNA replication. *Mol. Cell. Biol.* **14,** 923–933
56. Lauwers, E., Erpapazoglou, Z., Haguenauer-Tsapis, R., and Andre, B. (2010) The ubiquitin code of yeast permease trafficking. *Trends Cell Biol.* **20,** 196–204
57. Merhi, A., and Andre, B. (2012) Internal amino acids promote Gap1 permease ubiquitylation via TORC1/Npr1/14-3-3-dependent control of the Bul arrestin-like adaptors. *Mol. Cell. Biol.* **32,** 4510–4522
58. Neklesa, T. K., and Davis, R. W. (2009) A genome-wide screen for regulators of TORC1 in response to amino acid starvation reveals a conserved Npr2/3 complex. *PLoS Genet.* **5,** e1000515
59. Van Dyke, N., Baby, J., and Van Dyke, M. W. (2006) Stm1p, a ribosome-associated protein, is important for protein synthesis in Saccharomyces cerevisiae under nutritional stress conditions. *J. Mol. Biol.* **358,** 1023–1031
60. Rotin, D., and Kumar, S. (2009) Physiological functions of the HECT family of ubiquitin ligases. *Nat. Rev. Mol. Cell Biol.* **10,** 398–409
61. Belgareh-Touze, N., Leon, S., Erpapazoglou, Z., Stawiecka-Mirota, M., Urban-Grimal, D., and Haguenauer-Tsapis, R. (2008) Versatile role of the yeast ubiquitin ligase Rsp5p in intracellular trafficking. *Biochem. Soc. Trans.* **36,** 791–796
62. Gupta, R., Kus, B., Fladd, C., Wasmuth, J., Tonikian, R., Sidhu, S., Krogan, N. J., Parkinson, J., and Rotin, D. (2007) Ubiquitination screen using protein microarrays for comprehensive identification of Rsp5 substrates in yeast. *Mol. Syst. Biol.* **3,** 116
63. Gajewska, B., Kaminska, J., Jesionowska, A., Martin, N. C., Hopper, A. K., and Zoladek, T. (2001) WW domains of Rsp5p define different functions: determination of roles in fluid phase and uracil permease endocytosis in Saccharomyces cerevisiae. *Genetics* **157,** 91–101
64. Hsu, P. P., Kang, S. A., Rameseder, J., Zhang, Y., Ottina, K. A., Lim, D., Peterson, T. R., Choi, Y., Gray, N. S., Yaffe, M. B., Marto, J. A., and Sabatini, D. M. (2011) The mTOR-regulated phosphoproteome reveals a mechanism of mTORC1-mediated inhibition of growth factor signaling. *Science* **332,** 1317–1322
65. Robitaille, A. M., Christen, S., Shimobayashi, M., Cornu, M., Fava, L. L., Moes, S., Prescianotto-Baschong, C., Sauer, U., Jenoe, P., and Hall, M. N. (2013) Quantitative phosphoproteomics reveal mTORC1 activates de novo pyrimidine synthesis. *Science* **339,** 1320–1323
66. Yu, Y., Yoon, S. O., Poulogiannis, G., Yang, Q., Ma, X. M., Villen, J., Kubica, N., Hoffman, G. R., Cantley, L. C., Gygi, S. P., and Blenis, J. (2011) Phosphoproteomic analysis identifies Grb10 as an mTORC1 substrate that negatively regulates insulin signaling. *Science* **332,** 1322–1326